

Electron Transfer as a Liquid Droplet Contacting a Polymer Surface

Fei Zhan, Aurelia C. Wang, Liang Xu, Shiquan Lin, Jiajia Shao, Xiangyu Chen,* and Zhong Lin Wang*



Cite This: <https://dx.doi.org/10.1021/acsnano.0c08332>



Read Online

ACCESS |



Metrics & More



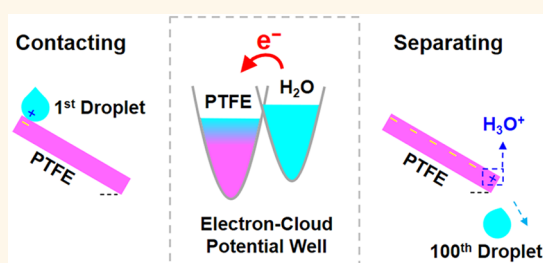
Article Recommendations



Supporting Information

ABSTRACT: It has been demonstrated that substantial electric power can be produced by a liquid-based triboelectric nanogenerator (TENG). However, the mechanisms regarding the electrification between a liquid and a solid surface remain to be extensively investigated. Here, the working mechanism of a droplet-TENG was proposed based on the study of its dynamic saturation process. Moreover, the charge-transfer mechanism at the liquid–solid interface was verified as the hybrid effects of electron transfer and ion adsorption by a simple but valid method. Thus, we proposed a model for the charge distribution at the liquid–solid interface, named Wang’s hybrid layer, which involves the electron transfer, the ionization reaction, and the van der Waals force. Our work not only proves that TENG is a probe for investigating charge transfer at interface of all phases, such as solid–solid and liquid–solid, but also may have great significance to water energy harvesting and may revolutionize the traditional understanding of the liquid–solid interface used in many fields such as electrochemistry, catalysis, colloidal science, and even cell biology.

KEYWORDS: contact electrification, triboelectric nanogenerator, liquid–solid, electron transfer, electric double layer, Wang’s hybrid layer



Water, covering over 70% of the Earth’s surface, could generate electric power that is 3 orders of magnitude higher than the global energy demand.^{1,2} Although traditional water energy harvesting technologies (for example, water turbines) have been employed for hundreds of years, only a very tiny portion of water energy is being utilized. Recently, some liquid-based electricity generators have emerged or have been improved along with the rapid development of nanostructured materials. Graphenes, carbon nanotubes, and other conductive materials have been used to interact with flowing, waving, dropping, and evaporating water to generate electricity.^{3,4} Their working mechanisms have all been interpreted by the electric double layer (EDL) model,^{5,6} where an electric potential layer is formed as a result of adsorbing a layer of ions on the solid surface followed by a gradient distribution of ions in liquid.

The triboelectric nanogenerator (TENG),^{7–9} based on the conjunction of contact electrification (CE) and electrostatic induction effect, was invented by Wang and co-workers in 2012. It is a powerful technology to convert randomly distributed, irregular, and wasted low-frequency energy into electric power. Moreover, a water-TENG,^{10–12} associated with the interaction between insulator and water, has been demonstrated to harvest water energy with high power density. For example, when a water droplet (100 μL) was released from a height of 15 cm and then came into contact with a polytetrafluoroethylene (PTFE) surface, 100 light-emitting diodes (LEDs) could be instantaneously lit up.¹³

Such superior electricity generation performance is related to the charge-transfer mechanism at the liquid–solid interface. Recently, Wang *et al.* have experimentally verified that the transferred charges are both electrons and ions in liquid-ceramic CE, and electron transfer can even dominate the CE between liquid and hydrophobic materials such as PTFE.^{14,15} Particularly, they have proposed a “two-step” model¹⁶ on the formation of an EDL, which is totally different from traditional understanding about the EDL. That is, electron transfer instantaneously occurs when liquid contacts a virgin solid surface (step 1) followed by counterion adsorption (step 2). More systematic studies are required to explore the detailed process regarding to charge-transfer process and its saturation status. The existence of surface ions at the initial state and their contributions to the liquid–solid CE need to be studied.

Here, those issues were investigated and resolved through a droplet-TENG, which generated electricity continuously when a sequence of liquid droplets contacted with and slid down a polymer surface and then slipped away. First, the dynamic saturation process of charge accumulation and surface potential

Received: October 4, 2020

Accepted: November 20, 2020



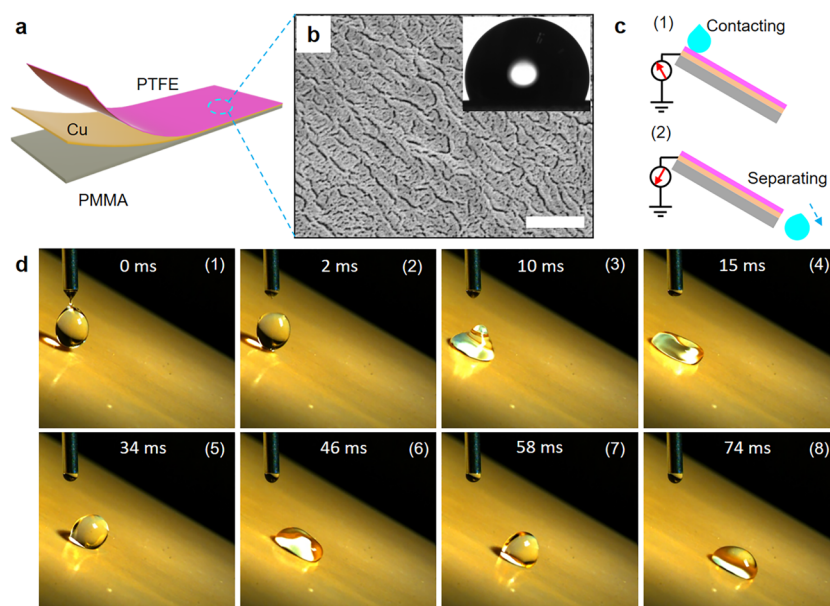


Figure 1. Experimental setup. (a) Structure of the droplet-TENG. PTFE film was attached on the top of the Cu electrode/PMMA substrate. (b) Scanning electron microscopy image and contact angle photo of the PTFE film. Scale bar: $1\ \mu\text{m}$. (c) Simple working mechanism of the droplet-TENG. (d) Snapshots showing the motion of a water droplet on the PTFE film. The droplet height was set at $0.6\ \text{cm}$.

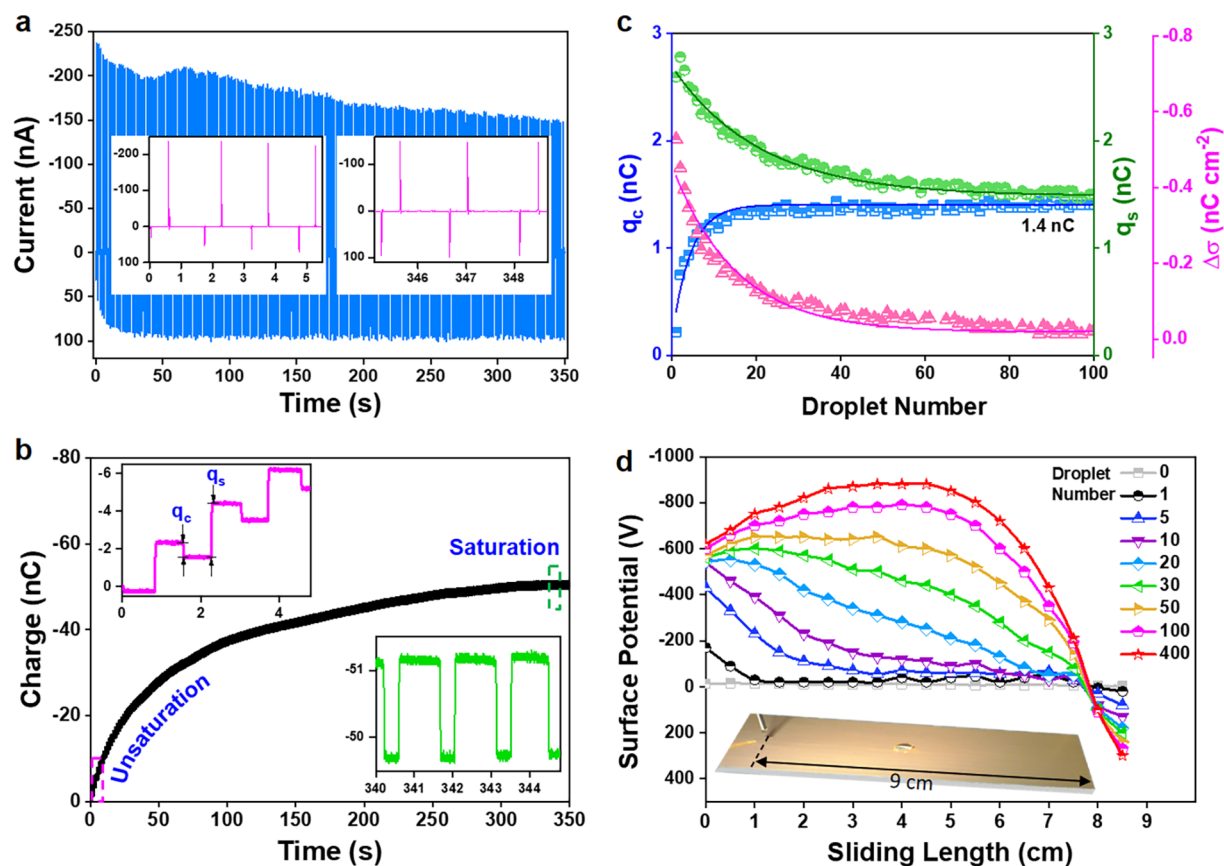


Figure 2. Electricity generation performance of PTFE film and hundreds of sequential water droplets. (a,b) Current and charge (Q) recorded by an electrometer. $Q = \sum(q_c - q_s)$, where q_c and q_s refer to the induced charge at the contacting or separating process of one droplet, respectively. Insets: Enlarged views that show the (a) current and (b) charge at the unsaturation ($q_c < q_s$) and the dynamic saturation state ($q_c = q_s$), respectively. The marked q_c and q_s refer to the second droplet. (c) q_c , q_s , and transferred charge density σ , $\sigma = (q_c - q_s)/A\ \text{nC cm}^{-2}$, as a function of droplet number, which can be fitted by exponential equations. (d) Variation of surface potential distribution along with the sliding track.

distribution on the polymer surface was experimentally studied. Then, a simple and valid method was proposed to change the

initial state of the solid surface by soaking it in different ion-rich solutions in advance to verify the electron-transfer mechanism

and investigate the influence of adsorbed ions on liquid–solid CE. Finally, a different charge distribution structural model, named Wang’s hybrid layer, distinguished from EDL model, was proposed for the liquid–solid interface, which can provide breakthroughs for electrochemistry, catalysis, colloidal science, and even cell biology associated with the liquid–solid interface.

RESULTS AND DISCUSSION

Droplet-TENG. As depicted in Figure 1a, the droplet-TENG used in this study was simply a single-electrode TENG, which consisted of three layers: a PTFE film for contact electrification, a copper film for electrostatic induction, and a poly(methyl methacrylate) (PMMA) plate for support. PTFE was selected to be electrified by contacting with liquid droplets due to its high charge-generation capability and stability. Its surface morphology (roughness of about 20 nm) and water contact angle (115°) are shown in Figure 1b. It is a hydrophobic material due to its surface chemical property (rich fluorine groups) and proper surface roughness. Thus, water droplets can easily slide off an inclined PTFE film.

In this work, liquid droplets (about 25 μL per drop, with a dropping frequency of about 40 drops per minute) were released from a grounded stainless-steel needle (2 mm diameter) at a fixed height above the polymer surface with a tilted angle of 30°, as shown in Figure 1c,d. To reduce the effect of gravitational potential energy of droplets as well as the influence of liquid–gas CE, unless otherwise specified, the droplet height was set as 0.6 cm, which was slightly longer than the long axis length of the droplet hanging at the needle. At this height, the motion of a water droplet when it impinged on the polymer was recorded by a fast camera at the rate of 1000 frames per second. Figure 1d shows the selected snapshots of a water droplet impinging on the polymer surface. When the water droplet completely separated from the grounded needle, it instantly came into contact with the polymer surface. The Weber number^{17,18} here is as low as 1.2 (see more details in the Supporting Information). The water droplet did not break up and did not detach from the hydrophobic surface during the impact and bouncing processes, as demonstrated in Figure 1d. Upon touching the surface at $t = 2$ ms, the drop partially spread to become cone-like (10 ms) and immediately followed with basin-like (15 ms) shapes and then recoiled back (34 ms) and started to slide down on the surface (in a stand-up and sit-down style) until detached from its end.

Dynamic Saturation Process. The induced current and charges from the interaction between a sequential of DI water droplets (18.2 M Ω cm) and fresh PTFE polymers were measured in the single-electrode mode¹⁹ in which only the copper electrode was connected to a grounded electrometer, as shown in Figure 2a,b. The values of the current peak and the induced charges for one droplet at contacting and separating were denoted as j_c , q_c and j_s , q_s , respectively. When the first DI water droplet left the grounded needle and fell on the polymer surface, a small j_c of 31 nA (Figure 2a) and small q_c of 0.2 nC (Figure 2b) were observed. Then, as the droplet separated from the polymer surface, a high j_s of 237 nA (negative current) and high q_s of 2.6 nC (negative charge) were recorded. This indicated that a negative charge of 2.4 nC was deposited on the PTFE surface as a result of single droplet contact; at the same time, an equal amount of positive charges was retained in the first water droplet, as demonstrated in Figure S1.

As the droplet number increased, the accumulated negative charges on the polymer surface alternatively and asymmetrically decrease (at contacting) and increase (at separating) until

reaching a saturation. As seen from Figure 2a–c, during the unsaturation stage, j_c and q_c increased gradually, while j_s and q_s decreased slowly as the droplet number increased periodically. The average charge density for each droplet ($\Delta\sigma$, nC cm⁻²) was calculated over all of the droplet sliding track ($A = 0.5 \times 9$ cm²), that is, $\Delta\sigma = (q_c - q_s)/A$. For the 100th droplet (corresponding to about 150 s in Figure 2a,b), $\Delta\sigma = 0.02$ nC cm⁻². Then during the saturation stage, those five quantities (j_c , q_c , j_s , q_s , $\Delta\sigma$) almost remain constant ($q_c = q_s$, $\Delta\sigma \approx 0$), indicating that dropping more droplets can hardly increase the surface charges on the insulator. This is supported by the results that the positive charge carried on one water droplet decreases to about 0.1 nC after about 80 droplets (Figure S1). Therefore, the charge curve in Figure 2b seemed like a square wave. Finally, the saturated charge, namely, the sum of ($q_c - q_s$), on the surface was approximately 51 nC. It was thus estimated that the average distance between two adjacent transferred charges on the solid surface was 37.6 nm, indicating a sparse distribution of the charges. Note that, although $q_c = q_s$ at saturation, j_c was not equal to j_s because the contact speed and separation speed were different. Moreover, as shown in Figure S2, the time-dependent current curve varied with the dynamics of a water droplet. As soon as the droplet touched the solid surface, the value of the current began to increase. In less than 10 ms, the current reached the peak value at which the droplet spread out to the maximum extent. Subsequently, the drop rebounded in about 20 ms, and thus the current decreased until reaching zero.

In addition, the value of the saturated charges strongly depends on the droplet height. Shown in Figure S3, when the distance between the drop-point and the end of the flat needle was less than 0.58 cm, the saturated charge was equal to 33 nC. In this condition, one water droplet contacted with the solid first and then separated from the grounded-needle made of stainless steel. Therefore, part of the generated charges may be compensated by the ground. To avoid those situations as well as to weaken the influences of gravity and air, the distance was set to 0.6 cm for all of the experiments in this work if not otherwise specified. Noting that, as the droplet height slightly increased from 0.6 cm ($We = 1.2$) to 0.7 cm ($We = 2.4$), the saturated charges increased more than 3-fold. Such a performance improvement may be due to the increments of Weber number and actual contact area. Since the surface of PTFE is not an atomically flat surface, the actual contact area can be directly increased by increasing the interface pressure between a liquid and a solid.

Surface Potential Distribution. To further understand the dynamic saturation process of liquid–solid CE, the surface potential distribution upon the sliding track on the insulator was measured by a noncontact electrometer. As shown in Figure 2d, after the first DI water droplet came into contact with, slid on, and then separated from the polymer, the increased negative surface potential mainly concentrated in the initial contact region (0 to 1 cm in the sliding length). This indicated that the charge-transfer process for the first droplet mainly occurred in the impinged region and then almost vanished in the following sliding surface, which may be simply because the positive surface charges on the droplet had reached saturation. As the droplet number increased, surface potential increased first at the upstream and then expanded to the downstream, similar to a spreading wave. On the other hand, as the droplet number increased, the growth rate of potential decreased significantly. For the impinged region, it almost stopped increasing after the 20th droplets, representing the saturation condition there. This

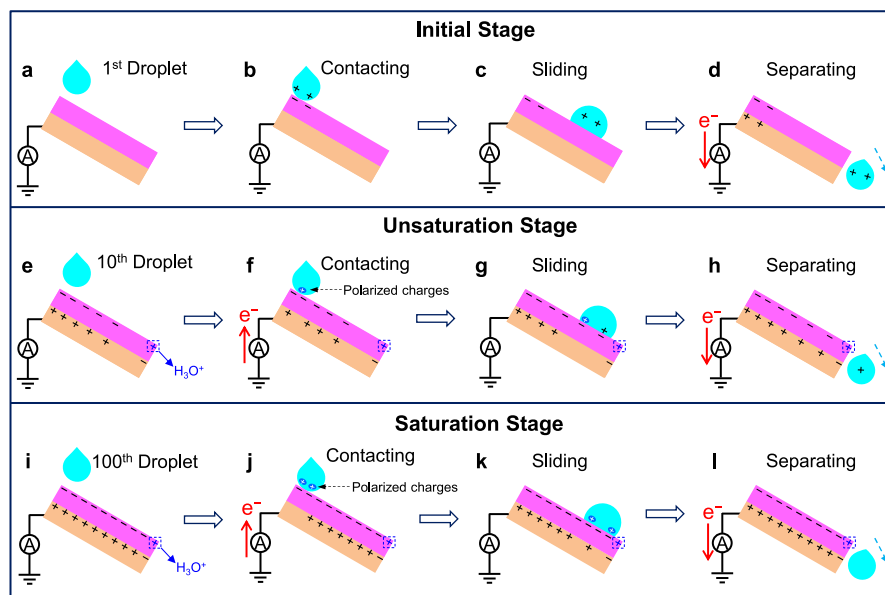


Figure 3. Working mechanism of the droplet-TENG. Three stages: initial, unsaturation, and saturation stages are included. (a–d) For the first droplet, negative charges are deposited at the impinging region on the insulator surface due to contact electrification, but the electrical signals (negative current and charge) are generated due to electrostatic induction as the droplet separates from the solid. (e–h) During the unsaturation stage, behaviors of contact electrification and electrostatic induction as well as the reversal phenomenon are exhibited. Positive and negative current (or charge) are produced as the sequential droplets come into contact with and then separate from the polymer, respectively. (i–l) After a large number of droplets fall on the insulator, the charge on it achieves saturation, and thus the generated electrical signals are contributed totally from the effects of electrostatic induction.

was consistent with the results shown in Figure 2c, where q_c nearly reached a constant value at that moment. Those results reveal that the dynamic saturation process of the CE between multidroplets and a polymer involves a sequential saturation process of the amount of charges on the polymer surface from the front to the end of the sliding track.

Notably, as shown in Figure 2d, charges almost did not transfer between an uncharged polymer surface and a water droplet with saturated positive charges (for example, the first water droplet) or between an uncharged water droplet and a polymer surface with saturated negative charges (for example, the 100th droplet). This phenomenon is able to be interpreted by the “electron-cloud potential well” model,²⁰ in which the electron transfer in CE is considered to be induced by the overlap of electron clouds of two atoms or two molecules. As illustrated in Figure S4a, if the charges of either PTFE or H₂O are saturated, their occupied energy levels of electrons are equal, thus electrons should not transfer between them. However, when uncharged PTFE comes into contact with uncharged H₂O, electrons are able to hop from the latter to the former (Figure S4b). This also can be understood from the three dimensionally electrostatic potential maps of C₃₀F₆₂ (simulating PTFE) and H₂O, calculated by the density functional theory (DFT) method, as shown in Figure S5. Blue and red regions refer to the regions of positive and negative potentials and correspond to the electron-poor and electron-rich regions, respectively. Obviously, electrons concentrate on the oxygen atom in one H₂O, whereas they are deficient at some regular sites on the PTFE. Hence, when a fresh water molecular comes into contact with fresh PTFE, it is highly possible to transfer an electron from water to PTFE.

However, by surprise, we found a “reversal phenomenon” in which the surface potential turned from negative to positive at the end of the sliding track, even at a saturation state (Figure 2d).

This indicated that positive charges were indeed dominant at the end of the sliding track. To understand this reversal phenomenon, effects of some experimental conditions such as sliding length, droplet height, air humidity, as well as materials type were investigated. Results shown in Figures S6 and S7 indicated that the reversal phenomenon may have little relationship with the length of the liquid sliding track and the nature of the polymer, as it remained occurring for a sliding length of 14 cm and for another polymer material such as fluorinated ethylene propylene. However, the droplet height and the air humidity indeed have significant effects on the reversal phenomenon, as demonstrated in Figures S7 and S8. The surface potential at the end tended to be negative at higher droplet height or lower air humidity. Such results suggest that the reversal phenomenon is associated with the residual water molecules on the solid surface at the end of the sliding track under a condition of very low droplet height and slightly high air humidity.

To gain an in-depth understanding about this, we should identify the nature of the positively charged water; namely, what will happen after a water molecule loses an electron, which has been rarely mentioned in the previous work regarding the liquid–solid CE. Here, we suppose that when a water molecular comes into contact with a virgin solid surface, it transfers an electron to the solid and thus itself becomes a cationic hole (H₂O⁺) in a quite short lifetime (less than 50 fs according to the latest report²¹), illustrated in Figure S9. Immediately, the H₂O⁺ cation joins with a neighboring water molecule to yield an OH radical and H₃O⁺, according to the primary chemical reaction of the ionization of liquid water:²² H₂O⁺ + H₂O → OH + H₃O⁺. Therefore, we suggest that the reversal phenomenon at the end of polymer, occurring under the conditions of a very low droplet height and slightly high air humidity, is likely to be the residual of hydrated protons (H₃O⁺) on the surface.

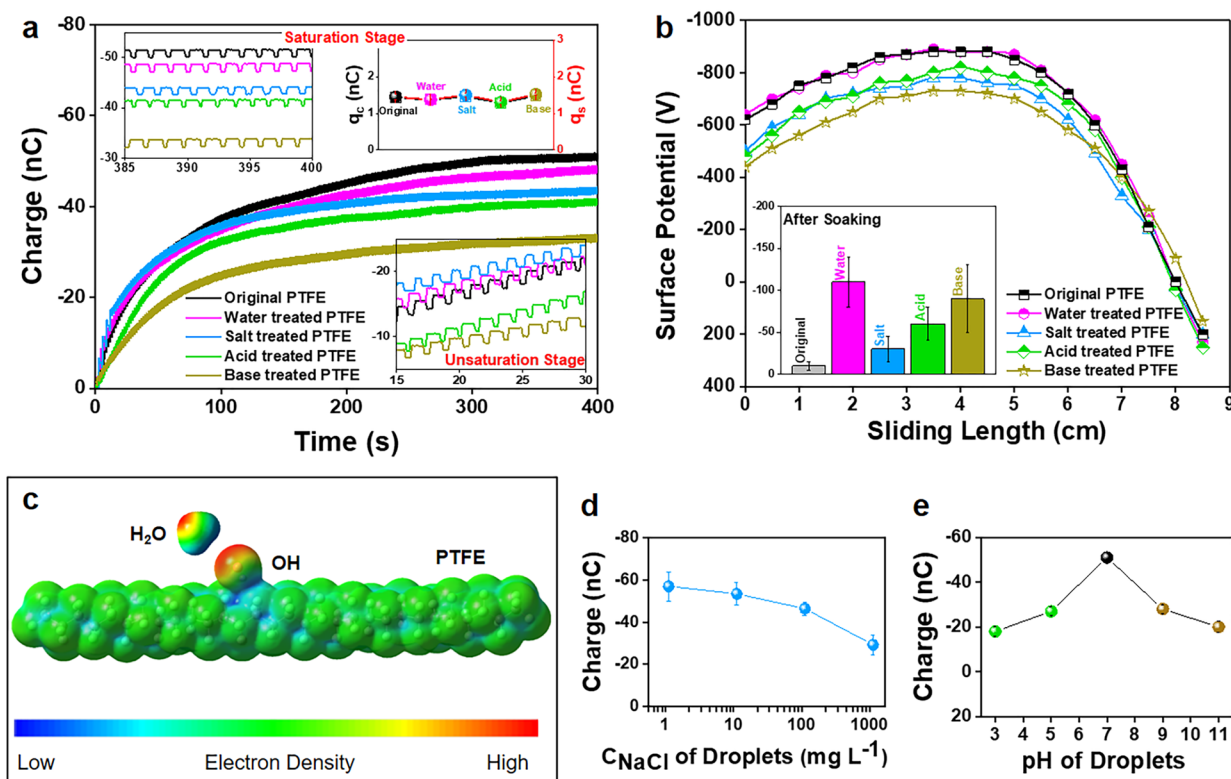


Figure 4. Contact electrification between DI water droplets and the soaked PTFE. (a) Charge generated from the interaction between water droplets and the original PTFE or the treated PTFE that was soaked in pure water, salt (1 g L^{-1} NaCl solution), acid (HCl solution, pH 3), or base (NaOH solution, pH 11). Both q_c and q_s at saturation stages for the original or treated PTFE films with different solutions were almost identical. (b) Surface potential distribution for the sliding track on the polymer after 400 water droplets interacted with the original or the treated PTFE. Inset: Surface potential of PTFE after different soaking treatments. (c) 3D plots of the molecular electrostatic potential map of $C_{30}F_{62}$ (simulating PTFE) with a deposited OH group and H_2O obtained from the DFT method. (d) Amount of cumulative charges of the original PTFE and NaCl droplets with different concentration (C_{NaCl}). (e) Amount of cumulative charges of the original PTFE and HCl/NaOH droplets with different pH.

Working Mechanism of the Droplet-TENG. Collectively, a more precise and comprehensive working mechanism of the droplet-TENG involving the dynamic process of charge accumulation starting from the initial state to the saturated state is proposed in Figure 3. Initially, when the first fresh water droplet falls down and contacts an uncharged polymer film, it deposits negative charges on the impinging region and makes itself positively charged (with excess H_3O^+), but the whole system maintains electrical neutral (Figure 3b,c). Then, when the droplet separates from the lower end of the solid, an instantaneous negative current and charge are established in the short-circuit case; that is, the metal electrode loses electrons to ground to screen the static charges on the polymer surface (Figure 3d). Starting with the second droplet, uncharged water droplets interact with the solid surface that has negative charges in some regions. As a result, the electrostatic induction (partial water molecules are polarized in the electric field) and contact electrification effects (charges continue to transfer at some unexplored interfaces) coexist during the unsaturation stage. Figure 3f,g shows the case of the 10th droplet that involves the effect of electrostatic induction in the upstream (polarized charges in water), the contact electrification effect in the downstream, as well as the reversal phenomenon at the end (due to the residual H_3O^+). Consequently, a positive current/charge and a negative current/charge develop as the droplet contacts and leaves the polymer surface, respectively. This is consistent with the results shown in Figure 2c, where q_c increases while q_s

gradually decreases until reaching a steady state, and the growth rate of q_c is higher than the decay rate of q_s because it is earlier for the impinging region to attain a charge saturation state than the downstream surface. Finally, during the saturation stage (Figure 3i–l), the surface charge density on the solid can hardly increase, and the current and charge signals are entirely derived from the effect of electrostatic induction. In this status, $q_c = q_s$ and the charge curve shows a square wave (Figure 2b).

“Soaking–Dropping” Experiments. To demonstrate the role of electron transfer and to investigate the influence of the existing ions that were on the solid surface at the initial state, on a liquid–polymer CE, a group of simple but valid “soaking–dropping” experiments were conducted, in which PTFE films were first soaked in solutions to fully absorb ions and then electrified with DI water droplets to compare their final saturated charges as well as surface potentials. The soaking process with different ion-rich solutions can maximize the possibility of ion adsorption, which can possibly change the initial state for liquid–solid CE.

Fresh PTFE films were slowly immersed into salt (1 g L^{-1} NaCl), acid (HCl, pH 3), and base (NaOH, pH 11) aqueous solutions for 0.5 h, which was believed to be enough to completely adsorb ions. They were also immersed in DI water for controlled experiments. Then, the soaked PTFE films were slowly separated from those liquids and naturally dried in a clean space for another 0.5 h to evaporate water to the greatest possible extent under the circumstance of 30% air humidity. As a

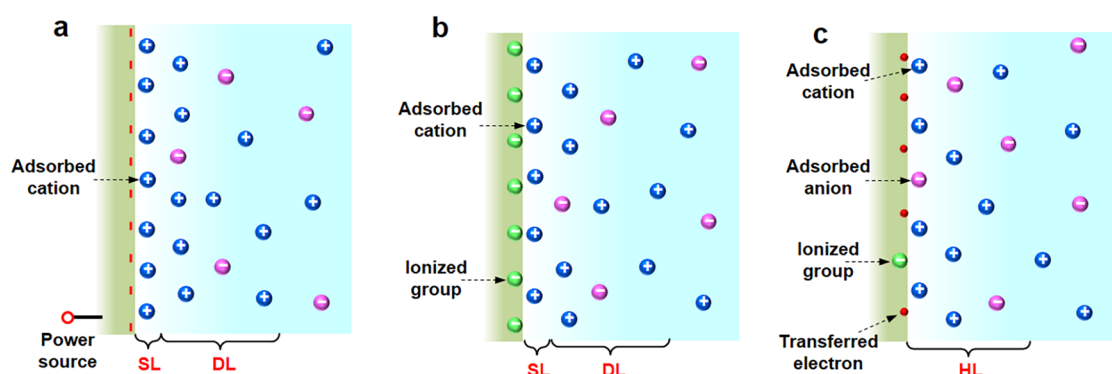


Figure 5. Charge distribution at a liquid–solid interface. (a,b) Electric double layer model according to the classical Gouy–Chapman–Stern theory for a liquid and (a) a charged or (b) an ionized solid material. The term “double layer” is constituted by the Stern layer, in which counterions are compactly arranged near the surface, and the diffuse layer, in which the concentration of counterions decays with distance from the surface. (c) Wang’s hybrid layer model toward the interface between a liquid and a solid (often a polymer). The hybrid layer contains adsorbed cations due to the attraction from transferred electrons, ionized surface groups, and adsorbed anions due to the van der Waals force.

result, ions were deemed to have deposited on the surface of the soaked PTFE films as much as possible. Note that those soaking treatments did not noticeably change the chemical properties, micromorphology, and water contact angle of PTFE, as demonstrated in Figures S10 and S11.

The surface potentials of the soaked PTFE films were measured. As can be seen from the inset in Figure 4b, the negative surface potential of those immersed in the DI water was not lower than that of those in the base solution, although the ion concentration of OH^- in the former was 4 orders of magnitude lower than that in the latter. This indicated that the transferred charges of the water–PTFE CE were probably dominated by electron transfer. In addition, likely due to the scarcity of hydroxide ions and the suppression of electron transfer by the ions in salt and acid solutions, the surface potential of the PTFE films treated with salt or acid solutions was also negative but lower than those in either water or the base.

Noticeably, the accumulated transferred charge was still high for the CE between water droplets and the base-treated PTFE, as shown in Figure 4a. The saturated charge (for 250 droplets) of the base-treated PTFE was about 70% of the original PTFE (untreated sample). Moreover, when water droplets were replaced with the base droplets (NaOH, pH 11) to interact with the base-treated PTFE, the saturated charge decreased (Figure S13). Thus, the electron transfer is probably dominated in the water–PTFE CE. Additionally, hydroxide ions (with the size of 0.11 nm) previously deposited on the base-treated PTFE could affect the CE by hindering the transferred electrons in the form of changing the polarity direction of water molecules at the interface. As shown in the 3D electrostatic potential map in Figure 4c, the deposited OH groups on the simulated PTFE are likely to repel the electron-rich region in a water molecular. As a result, the existence of ions on the solid surface at the initial state probably weakened the subsequent liquid–solid CE by suppressing the degree of electron transfer, although it was dominant.

After about 400 droplets were sequentially contacted with, slid on, and separated from the treated PTFE surface, the saturated surface potentials were measured and compared in Figure 4b. The saturated surface negative potentials for the original PTFE and the water-treated PTFE were almost overlapped, whereas those for salt- or acid-treated PTFE were slightly lower. Specifically, for the NaOH-treated PTFE,

probably due to the repulsion effect of hydroxide ions to electron transfer, the surface negative potential was the weakest in the upstream of the sliding track. However, it appeared stronger downstream; in other words, the reversal phenomenon (from negative to positive) appeared nearer to the edge of the solid, which may be attributed to the neutralization effect between the residual hydronium ions and the previously adsorbed hydroxide ions during the soaking treatment process.

In addition to the CE between PTFE and DI water droplets, the experiments with ion-rich droplets such as salt, acid, or base droplets were also conducted. As can be seen from Figure 4d, the saturation charges on PTFE decreased as the concentration of NaCl droplets increased, which was consistent with the previous report.^{14,15} The more salt ions in a liquid, the less charges are transferred at the interface between the salt solution and a solid. This conclusion was also suitable for the cases of acid/base droplets, as demonstrated in Figure 4e. The stronger the acidity or alkalinity of the solution, the lower the saturation charge.

Therefore, electron transfer is probably dominant in the case of CE between water and a polymer. Regardless if there are ions in a liquid or on a solid surface, electron transfer still occurs in the subsequent liquid–solid CE, indicating that liquid–solid CE is a hybrid effect including both ion adsorption and electron transfer. Additionally, the hydroxide ions on the solid surface at the initial state can weaken the subsequent liquid–solid CE to some extent.

Wang’s Hybrid Layer. The charges and potential distribution at the liquid–solid interface are commonly described by the EDL model based on the Gouy–Chapman–Stern theory.^{5,23} Figure 5a shows the classical EDL structure at the interface of an electrode (an electrical conductor or a polarized material) and an electrolyte (an ion-rich aqueous solution or an ionic liquid). It consists of the Stern layer where ions (often hydrated) are strongly adsorbed on the charged electrode, and the diffuse layer, where the concentration of counterions decreases with distance away from the surface. This picture is commonly employed in the electrochemical related fields such as supercapacitors,²⁴ water splitting,²⁵ capacitive deionization,^{26,27} hydrogel ionotronics,^{28,29} electric double layer transistors,³⁰ and electrowetting.^{31,32} In addition, for a solid material with abundant chemical groups that intends to be positively charged or negatively charged through the reactions of ionization or dissociation with a liquid, such as a carbon material with carboxylic groups ($-\text{COOH}$), counterions can be attracted

to and adsorbed onto the solid surface that is decorated with abundant ionized groups (for example, $-\text{COO}^-$), as illustrated in Figure 5b. This EDL picture is commonly used in colloidal science,³³ cell biology, as well as in energy harvesting fields such as capacitive mixing.^{34,35}

However, the electron transfer that is particularly derived from the liquid–insulator CE is not considered in the formation of the classical EDL model. Herein, we put forward a hybrid layer model for the interface between a liquid and a solid (Figure 5c). When the material, tending to be negatively charged in the triboelectric series, comes into contact with an aqueous solution, some sites on the solid surface can obtain electrons from water molecules and then attract cations, whereas other sites can be covered with specifically adsorbed anions³⁶ due to the van der Waals force, which is a universal effect. If a solid is chemically active in a liquid (for example, SiO_2 in water), ionized groups also need to be considered. Such a complex interface structure is named Wang's hybrid layer that considers the influences of the electron transfer, the ionization reaction, and the van der Waals force. This model is proposed based on our understanding that both electrons and ions are transferred during liquid–solid CE, which has been demonstrated in this work. It is recommended to be used for applications including but not limited to liquid-TENG and biomedical areas such as neural science and intercellular information transfer.

CONCLUSIONS

In summary, the dynamic process of charge accumulation, the mechanism of charge transfer for liquid–solid CE, as well as the charge distribution at the liquid–solid interface have been extensively studied *via* a droplet-TENG, where multiple droplets contact with, slide down, and then separate from a hydrophobic polymer surface. The results of the dynamic saturation study may have great significance to water-related energy harvesting technologies.

The electron-transfer mechanism on the liquid–solid CE was verified. More importantly, the “electron-cloud potential well” model can interpret all of the experimental phenomena, including the CE vanishing when the liquid or/and the solid achieves saturation. The details are as follows:

1. The soaking experiments with different ion-rich solutions can maximize the possibility of ion adsorption. However, CE still occurred between water and treated polymer films that were previously soaked in ion-rich solutions, which suggests that the ion adsorption is not the dominating factor for this water–polymer CE.
2. The potential change on the soaked polymer surface using water was not lower than that soaked with base solution, which indicates that the high ion concentration cannot enhance the CE.
3. The saturated charges derived from a polymer and ion-rich droplets were lower than those from the polymer and pure water droplets. It means that the existence of ions may interfere with the electron-transfer process, thus leading to a suppression of the total CE.
4. Positive charges can exist at the end of the sliding track due to the residual of hydronium, which can answer a key question on what will happen after a water molecule loses an electron in liquid–solid CE.

Finally, a model named Wang's hybrid layer is proposed to understand the intrinsic charge distribution at the liquid–solid interface. Our model involves the electron transfer, the

ionization reaction, and the van der Waals force, which may revolutionize the traditional understanding about the liquid–solid interface, which is the foundation of electrochemistry, catalysis, colloidal science, and even cell biology.

METHODS

Fabrication of Droplet-TENG. The PTFE film is ASF-110 FR (thickness = 80 μm) bought from Chukoh Company (Japan). Before every experiment, the films were rinsed with ethanol, and their surface potential should be below 15 V. The films were carefully attached onto smooth copper films with a thickness of 500 μm . Smooth and clean PMMA plates ($6 \times 16 \times 0.5 \text{ cm}^3$) were used as the backboards. Note that the adhered PTFE films must cover all of the areas of the copper films to avoid the electrical interference from droplets to copper and avoid the chemical corrosion of copper in solutions.

Characterization. The surface morphology of the materials was observed using a scanning SU8020 cold-field scanning electron microscope. Their structure was obtained by a Fourier transform infrared spectrophotometer (VERTEX80v). The roughness and the contact angle came from a step meter (KLA-TencorP7) and a contact angle measuring machine (CA100C), respectively.

Electrical Measurement. All of the induced current and charges of the copper electrode derived from the interaction of droplets and the polymer were measured by connecting the electrode with a Keithley 6517b electrometer with a Labview program on a computer. When one droplet falls on or is separated from the polymer's surface, a current peak or a charge stage appears on the Labview interface. Those data are deemed to correspond to the charge variation on the polymer surface. The excess charge on a droplet that separated from the polymer was measured by a nanocoulomb meter (model 284, Monroe Electronics, USA). The surface potential was measured with a TREK 347 electrostatic voltmeter without physical contact. The probe-to-surface distance was set as 1 mm. Notably, unless otherwise specified, the tested devices were made of PTFE; the sliding length was 9 cm; the droplet height was 0.6 cm; and the air humidity was 30%.

ASSOCIATED CONTENT

Supporting Information

The Supporting Information is available free of charge at <https://pubs.acs.org/doi/10.1021/acsnano.0c08332>.

Experimental results of varying the droplet height, sliding length, and air humidity; 3D plots of the molecular electrostatic potential map; characterizations of the treated PTFE; comparison between EDL model and our hybrid layer model (PDF)

AUTHOR INFORMATION

Corresponding Authors

Xiangyu Chen – Beijing Institute of Nanoenergy and Nanosystems, Chinese Academy of Sciences, Beijing 100083, China; School of Nanoscience and Technology, University of Chinese Academy of Sciences, Beijing 100049, China; orcid.org/0000-0002-0711-0275; Email: chenxiangyu@binn.cas.cn

Zhong Lin Wang – Beijing Institute of Nanoenergy and Nanosystems, Chinese Academy of Sciences, Beijing 100083, China; School of Nanoscience and Technology, University of Chinese Academy of Sciences, Beijing 100049, China; School of Materials Science and Engineering, Georgia Institute of Technology, Atlanta, Georgia 30332-0245, United States; orcid.org/0000-0002-5530-0380; Email: zlwang@gatech.edu

Authors

Fei Zhan – Beijing Institute of Nanoenergy and Nanosystems, Chinese Academy of Sciences, Beijing 100083, China; School of Nanoscience and Technology, University of Chinese Academy of Sciences, Beijing 100049, China

Aurelia C. Wang – School of Materials Science and Engineering, Georgia Institute of Technology, Atlanta, Georgia 30332-0245, United States

Liang Xu – Beijing Institute of Nanoenergy and Nanosystems, Chinese Academy of Sciences, Beijing 100083, China; School of Nanoscience and Technology, University of Chinese Academy of Sciences, Beijing 100049, China

Shiquan Lin – Beijing Institute of Nanoenergy and Nanosystems, Chinese Academy of Sciences, Beijing 100083, China; School of Nanoscience and Technology, University of Chinese Academy of Sciences, Beijing 100049, China

Jiajia Shao – Beijing Institute of Nanoenergy and Nanosystems, Chinese Academy of Sciences, Beijing 100083, China; School of Nanoscience and Technology, University of Chinese Academy of Sciences, Beijing 100049, China

Complete contact information is available at:
<https://pubs.acs.org/10.1021/acsnano.0c08332>

Author Contributions

F.Z., X.C., and Z.L.W. planned the study. F.Z. conducted the experiments and simulations. F.Z., A.C.W., L.X., S.L., J.S., X.C., and Z.L.W. wrote the manuscript. All the authors discussed the results and commented on the manuscript.

Notes

The authors declare no competing financial interest.

ACKNOWLEDGMENTS

Research was supported by the National Key R&D Project from Minister of Science and Technology (2016YFA0202704), National Natural Science Foundation of China (Grant Nos. 51775049, 51605033, 51432005, 5151101243, and 51561145021), Beijing Municipal Science & Technology Commission (Z171100000317001, Z171100002017017, Y3993113DF, 4192069, and 2017000021223ZK03), and China Postdoctoral Science Foundation (No. 2019M660585). We would like to thank Yuxiang Shi, Dr. Wei Zhong, Dr. Jin Hui Nie, Prof. Cheng Xu, Prof. Tao Jiang, Prof. Wei Tang, Jie An, and Xiu Zhong Zhao for helpful discussions.

REFERENCES

- (1) Zhang, Z.; Li, X.; Yin, J.; Xu, Y.; Fei, W.; Xue, M.; Wang, Q.; Zhou, J.; Guo, W. Emerging Hydrovoltaic Technology. *Nat. Nanotechnol.* **2018**, *13*, 1109–1119.
- (2) Wang, Z. L.; Jiang, T.; Xu, L. Toward the Blue Energy Dream by Triboelectric Nanogenerator Networks. *Nano Energy* **2017**, *39*, 9–23.
- (3) Liu, A. T.; Zhang, G.; Cottrill, A. L.; Kunai, Y.; Kaplan, A.; Liu, P. W.; Koman, V. B.; Strano, M. S. Direct Electricity Generation Mediated by Molecular Interactions with Low Dimensionality Carbon Materials-A Mechanistic Perspective. *Adv. Energy Mater.* **2018**, *8*, 1802212.
- (4) Xue, G. B.; Xu, Y.; Ding, T. P.; Li, J.; Yin, J.; Fei, W. W.; Cao, Y. Z.; Yu, J.; Yuan, L. Y.; Gong, L.; Chen, J.; Deng, S. Z.; Zhou, J.; Guo, W. L. Water-Evaporation-Induced Electricity with Nanostructured Carbon Materials. *Nat. Nanotechnol.* **2017**, *12*, 317–321.
- (5) Fedorov, M. V.; Kornyshev, A. A. Ionic Liquids at Electrified Interfaces. *Chem. Rev.* **2014**, *114*, 2978–3036.
- (6) Favaro, M.; Jeong, B.; Ross, P. N.; Yano, J.; Hussain, Z.; Liu, Z.; Crumlin, E. J. Unravelling the Electrochemical Double Layer by Direct Probing of the Solid/Liquid Interface. *Nat. Commun.* **2016**, *7*, 12695.
- (7) Fan, F. R.; Tian, Z. Q.; Wang, Z. L. Flexible Triboelectric Generator! *Nano Energy* **2012**, *1*, 328–334.
- (8) Wang, Z. L. Triboelectric Nanogenerator (TENG)-Sparking an Energy and Sensor Revolution. *Adv. Energy Mater.* **2020**, *10*, 2000137.
- (9) Hinchet, R.; Yoon, H. J.; Ryu, H.; Kim, M. K.; Choi, E. K.; Kim, D. S.; Kim, S. W. Transcutaneous Ultrasound Energy Harvesting Using Capacitive Triboelectric Technology. *Science* **2019**, *365*, 491.
- (10) Tang, W.; Chen, B. D.; Wang, Z. L. Recent Progress in Power Generation from Water/Liquid Droplet Interaction with Solid Surfaces. *Adv. Funct. Mater.* **2019**, *29*, 1901069.
- (11) Chatterjee, S.; Burman, S. R.; Khan, I.; Saha, S.; Choi, D.; Lee, S.; Lin, Z.-H. Recent Advancements in Solid-Liquid Triboelectric Nanogenerators for Energy Harvesting and Self-Powered Applications. *Nanoscale* **2020**, *12*, 17663–17697.
- (12) Moon, J. K.; Jeong, J.; Lee, D.; Pak, H. K. Electrical Power Generation by Mechanically Modulating Electrical Double Layers. *Nat. Commun.* **2013**, *4*, 1487.
- (13) Xu, W.; Zheng, H.; Liu, Y.; Zhou, X.; Zhang, C.; Song, Y.; Deng, X.; Leung, M.; Yang, Z.; Xu, R. X.; Wang, Z. L.; Zeng, X. C.; Wang, Z. A Droplet-Based Electricity Generator with High Instantaneous Power Density. *Nature* **2020**, *578*, 392–396.
- (14) Nie, J.; Ren, Z.; Xu, L.; Lin, S.; Zhan, F.; Chen, X.; Wang, Z. L. Probing Contact-Electrification-Induced Electron and Ion Transfers at a Liquid-Solid Interface. *Adv. Mater.* **2020**, *32*, 1905696.
- (15) Lin, S.; Xu, L.; Chi Wang, A.; Wang, Z. L. Quantifying Electron-Transfer in Liquid-Solid Contact Electrification and the Formation of Electric Double-Layer. *Nat. Commun.* **2020**, *11*, 399.
- (16) Wang, Z. L.; Wang, A. C. On the Origin of Contact-Electrification. *Mater. Today* **2019**, *30*, 34–51.
- (17) Sun, Q.; Wang, D.; Li, Y.; Zhang, J.; Ye, S.; Cui, J.; Chen, L.; Wang, Z.; Butt, H. J.; Vollmer, D.; Deng, X. Surface Charge Printing for Programmed Droplet Transport. *Nat. Mater.* **2019**, *18*, 936–941.
- (18) Bird, J. C.; Dhiman, R.; Kwon, H. M.; Varanasi, K. K. Reducing the Contact Time of a Bouncing Drop. *Nature* **2013**, *503*, 385.
- (19) Wu, C.; Wang, A. C.; Ding, W.; Guo, H.; Wang, Z. L. Triboelectric Nanogenerator: A Foundation of the Energy for the New Era. *Adv. Energy Mater.* **2019**, *9*, 1802906.
- (20) Xu, C.; Zi, Y. L.; Wang, A. C.; Zou, H. Y.; Dai, Y. J.; He, X.; Wang, P. H.; Wang, Y. C.; Feng, P. Z.; Li, D. W.; Wang, Z. L. On the Electron-Transfer Mechanism in the Contact-Electrification Effect. *Adv. Mater.* **2018**, *30*, 1706790.
- (21) Loh, Z. H.; Doumy, G.; Arnold, C.; Kjellsson, L.; Southworth, S. H.; Al Haddad, A.; Kumagai, Y.; Tu, M. F.; Ho, P. J.; March, A. M.; Schaller, R. D.; Bin Mohd Yusof, M. S.; Debnath, T.; Simon, M.; Welsch, R.; Inhester, L.; Khalili, K.; Nanda, K.; Krylov, A. I.; Moeller, S.; et al. Observation of the Fastest Chemical Processes in the Radiolysis of Water. *Science* **2020**, *367*, 179–182.
- (22) Gauduel, Y.; Pommeret, S.; Migus, A.; Antonetti, A. Some Evidence of Ultrafast H₂O⁺-Water Molecule Reaction in Femtosecond Photoionization of Pure Liquid Water - Influence on Geminate Pair Recombination Dynamics. *Chem. Phys.* **1990**, *149*, 1–10.
- (23) Stern, H. O. Zur Theorie der Elektrolytischen Doppelschicht. *Elektrochem.* **1924**, *30*, 508.
- (24) Zhang, L. L.; Zhao, X. S. Carbon-Based Materials as Supercapacitor Electrodes. *Chem. Soc. Rev.* **2009**, *38*, 2520–2531.
- (25) Stamenkovic, V. R.; Strmcnik, D.; Lopes, P. P.; Markovic, N. M. Energy and Fuels from Electrochemical Interfaces. *Nat. Mater.* **2017**, *16*, 57–69.
- (26) Wu, T.; Wang, G.; Dong, Q.; Zhan, F.; Zhang, X.; Li, S.; Qiao, H.; Qiu, J. Starch Derived Porous Carbon Nanosheets for High-Performance Photovoltaic Capacitive Deionization. *Environ. Sci. Technol.* **2017**, *51*, 9244–9251.
- (27) Srimuk, P.; Su, X.; Yoon, J.; Aurbach, D.; Presser, V. Charge-Transfer Materials for Electrochemical Water Desalination, Ion Separation and the Recovery of Elements. *Nat. Rev. Mater.* **2020**, *5*, 517–538.
- (28) Yang, C.; Suo, Z. Hydrogel Ionotronics. *Nat. Rev. Mater.* **2018**, *3*, 125–142.

- (29) Schroeder, T. B. H.; Guha, A.; Lamoureux, A.; VanRenterghem, G.; Sept, D.; Shtein, M.; Yang, J.; Mayer, M. An Electric-Eel-Inspired Soft Power Source from Stacked Hydrogels. *Nature* **2017**, *552*, 214.
- (30) Du, H.; Lin, X.; Xu, Z.; Chu, D. Electric Double-Layer Transistors: A Review of Recent Progress. *J. Mater. Sci.* **2015**, *50*, 5641–5673.
- (31) Mark, D.; Haeberle, S.; Roth, G.; von Stetten, F.; Zengerle, R. Microfluidic Lab-on-a-Chip Platforms: Requirements, Characteristics and Applications. *Chem. Soc. Rev.* **2010**, *39*, 1153–1182.
- (32) Quinn, A.; Sedev, R.; Ralston, J. Influence of the Electrical Double Layer in Electrowetting. *J. Phys. Chem. B* **2003**, *107*, 1163–1169.
- (33) Liang, Y.; Hilal, N.; Langston, P.; Starov, V. Interaction Forces between Colloidal Particles in Liquid: Theory and Experiment. *Adv. Colloid Interface Sci.* **2007**, *134–135*, 151–166.
- (34) Zhan, F.; Wang, G.; Wu, T. T.; Dong, Q.; Meng, Y. L.; Wang, J. R.; Yang, J.; Li, S. F.; Qiu, J. S. High Performance Asymmetric Capacitive Mixing with Oppositely Charged Carbon Electrodes for Energy Production from Salinity Differences. *J. Mater. Chem. A* **2017**, *5*, 20374–20380.
- (35) Zhan, F.; Wang, Z. J.; Wu, T. T.; Dong, Q.; Zhao, C. T.; Wang, G.; Qiu, J. S. High Performance Concentration Capacitors with Graphene Hydrogel Electrodes for Harvesting Salinity Gradient Energy. *J. Mater. Chem. A* **2018**, *6*, 4981–4987.
- (36) Zimmermann, R.; Dukhin, S.; Werner, C. Electrokinetic Measurements Reveal Interfacial Charge at Polymer Films Caused by Simple Electrolyte Ions. *J. Phys. Chem. B* **2001**, *105*, 8544–8549.